Hindawi
Mathematical Problems in Engineering
Volume 2022, Article ID 7804440, 11 pages
https://doi.org/10.1155/2022/7804440

Research Article

Microcontroller Implementation, Controls, and Synchronization of Three-Dimensional Autonomous System with a Parabolic Equilibrium Point

Tokoue Ngatcha Dianorre,[1] **Dongmo Eric Donald**,[2] **Metsebo Jules**,[3] **Nasr Saeed**,[4] **Kemnang Tsafack Alex Stephane**,[5] **and Boudoue Malwe Hubert**[6]

[1]*Department of Automotive and Mechatronics Engineering, National Higher Polytechnic School of Douala, University of Douala, Box 24, Douala 2701, Cameroon*
[2]*Department of Mechanical Engineering, College of Technology, University of Buea, P.O. Box 63, Buea, Cameroon*
[3]*Department of Hydraulics and Water Management, National Advanced School of Engineering, University of Maroua, P.O. Box 46, Maroua, Cameroon*
[4]*Department of Physics, College of Education, Nyala University, P.O. Box 155, Nyala, Sudan*
[5]*Research Unit of Condensed Matter of Electronics and Signal Processing, Department of Physics, Faculty of Sciences, University of Dschang, P.O. Box 67, Dschang, Cameroon*
[6]*Department of Physics, Faculty of Science, University of Maroua, P.O. Box 814, Maroua, Cameroon*

Correspondence should be addressed to Tokoue Ngatcha Dianorre; tokouengatcha1@gmail.com

Received 16 September 2022; Revised 25 October 2022; Accepted 5 November 2022; Published 21 November 2022

Academic Editor: Ernesto Zambrano-Serrano

The microcontroller implementation, controls, and synchronization of a three-dimensional (3D) autonomous system with a parabolic equilibrium point are investigated in this paper. The system in question displays a reverse period doubling route hidden chaotic attractors with two different shapes. Then, the partial and total amplitude controls of the system are achieved by inserting two parameters. A microcontroller implementation is performed in order to confirm the results obtained from the numerical simulations. It is found that the results from the numerical simulations and microcontroller implementation qualitatively agree with each other. The sliding mode controllers are designed to control chaos in the system under study. With the sliding mode control method, the numerical simulations confirm that chaos can be controlled in the 3D autonomous system with a parabolic equilibrium point. In addition, two chaotic 3D autonomous systems with a parabolic equilibrium point and the same parameters are synchronized by the use of a unidirectional linear error feedback coupling scheme. Finally, an active control technique is applied to bring about chaos synchronization between two chaotic 3D autonomous systems with a parabolic equilibrium and different parameters.

1. Introduction

Nowadays, chaos theory is one of the biggest paradigm shifts in the nonlinear dynamics of complex systems. Wide varieties of dynamical systems with chaos have been reported in many modelling applications thus in many fields such as mechanics, biology, chemistry, and electronics. The strong use of chaos has motivated researchers to come up with many new chaotic systems [1–8]. It is now evident from various studies that there exist uncommon chaotic systems with hidden attractors. Now, it is well established that no standard computational procedure can permit us to have a straightforward way of localizing hidden attractors. In chaos theory, hidden attractors are a very fascinating topic. The basin of attraction of hidden attractors does not intersect with small neighborhoods of any equilibrium points. This plays a very significant role in the fields of nonlinear circuits.

According to Leonov and Kuznetsov, periodic and chaotic attractors can either be categorized as self-excited or hidden [1]. While the basin of attraction of a self-excited attractor is associated with an unstable equilibrium, that of a hidden attractor does not intersect with small neighborhoods of any equilibrium points. Because it is important to enable a chaotic system to maintain a desirable dynamical behavior, techniques such as static or dynamic feedback control or an open-loop control method have been proposed to achieve this goal. In some recent cases, the major task is to investigate the state feedback control law in order to stabilize the system around its unstable equilibrium point. This has so far been done using the active control method [9, 10], the sliding mode control method [11, 12], the adaptive control method [13, 14], and the backstepping method [15, 16].

The foundation of science and engineering has been, in the past decades, impacted by the study of chaos with the discovery of chaos synchronization being one of the most exciting developments in recent times. Therefore, two coupled chaotic oscillators can be synchronized using the same methods as those used for controlling nonlinear systems. Pecora and Carroll [17] discovered that for synchronization of chaotic systems to be possible, an appropriate coupling design must be found, such that for instance, the chaotic time evolutions of the two systems become identical. The use of state observers or the use of control laws according to the Lyapunov stability theory is another technique by which chaotic systems can be synchronized. Synchronization can either be the phase synchronization [18], the complete synchronization [18, 19], the generalized synchronization [20], the antisynchronization [21], the generalized projective synchronization [22], the hybrid synchronization [23], the difference synchronization [15], or the difference-difference synchronization [16].

Inspired by these recent works [1, 24] and motivated by the great interest in hidden attractors and some discoveries about coexisting asymmetric attractors, we proposed a three-dimensional autonomous system with a parabolic equilibrium point. This chaotic system is then analyzed by phase portraits, time histories, and the Lyapunov exponent. We will use the sliding mode control method to control chaos in the proposed 3D autonomous system with parabolic equilibrium point. A study of synchronization of two identic proposed 3D autonomous systems with parabolic equilibrium point will be investigated by using unidirectional feedback linear and nonlinear coupling. By using a microcontroller, a circuit is designed and built to plot the different phase portraits.

The structure of the rest of this paper is as follows: the amplitude controls and microcontroller implementation of the proposed three-dimensional system with a parabolic equilibrium point are investigated in Section 2. Section 3 deals with the chaos control of a 3D system with a parabolic equilibrium point by using the sliding mode control method. In Section 4, a unidirectional linear error feedback coupling scheme is used to synchronize two chaotic autonomous 3D systems with a parabolic equilibrium point and the same parameters. In addition, an active control technique is employed to achieve chaos synchronization between chaotic 3D autonomous systems with a parabolic equilibrium point and different parameters. Finally, the paper is concluded in Section 5.

2. Amplitude Controls and Microcontroller Implementation of 3D Autonomous System with a Parabolic Equilibrium

A 3D autonomous system is proposed:

$$\frac{dx}{dt} = -z, \tag{1a}$$

$$\frac{dy}{dt} = xz^2, \tag{1b}$$

$$\frac{dz}{dt} = x - y^2 + z\left(ay^2 - z^2\right). \tag{1c}$$

With x, y, z being state variables, t the time, and a a positive parameter, the equilibrium point of system is parabolic with expression $E = \{(x, y, z) \in R^3/x = (y^*)^2, y = y^*, z = 0\}$. It is important to note that there is a difference between hyperbolic equilibrium point and parabolic equilibrium point. The hyperbolic equilibrium can be defined, for example, as $x = 1/(y^*)^n$ where n is an odd integer number while the parabolic equilibrium point can be defined, for example, as $x = (y^*)^k$ where k is an even integer number. At the parabolic equilibrium point E, the characteristic equation of system (1a)–(1c) is given by

$$\lambda\left[\lambda^2 - a\left(y^*\right)^2\lambda + 1\right] = 0. \tag{2}$$

The Routh–Hurwitz condition for the stability of this system at the parabolic equilibrium point E is $-a(y^*)^2 > 0$. Since $a > 0$, the parabolic equilibrium point E is always unstable. Figure 1 shows the plots of the dynamical behaviors of the 3D autonomous system with a parabolic equilibrium point.

Two different shapes of chaotic hidden attractors (see Figures 1(a) and 1(b)), period-4-oscillations (see Figure 1(c)), period-2-oscillations (see Figure 1(d)), and period-1-oscillations (see Figure 1(e)) are shown at $a = 3.05$, $a = 3.18$, $a = 3.22$, $a = 3.35$, and $a = 3.45$, respectively.

The amplitudes of the state variable x in system (1a)–(1c) can be partially controlled by making the change of variable $x \longrightarrow x + \beta$ in system (1a)–(1c) where β is the boosting controller. So, system (1a)–(1c) becomes:

$$\frac{dx}{dt} = -z, \tag{3a}$$

$$\frac{dy}{dt} = (x + \beta)z^2, \tag{3b}$$

$$\frac{dz}{dt} = (x + \beta) - y^2 + z\left(ay^2 - z^2\right). \tag{3c}$$

In this case, $E_1 = \{(x, y, z) \in R^3/x = \beta - (y^*)^2, y = y^*, z = 0\}$ is the parabolic equilibrium point of system (3a)–(3c). Its characteristic equation is

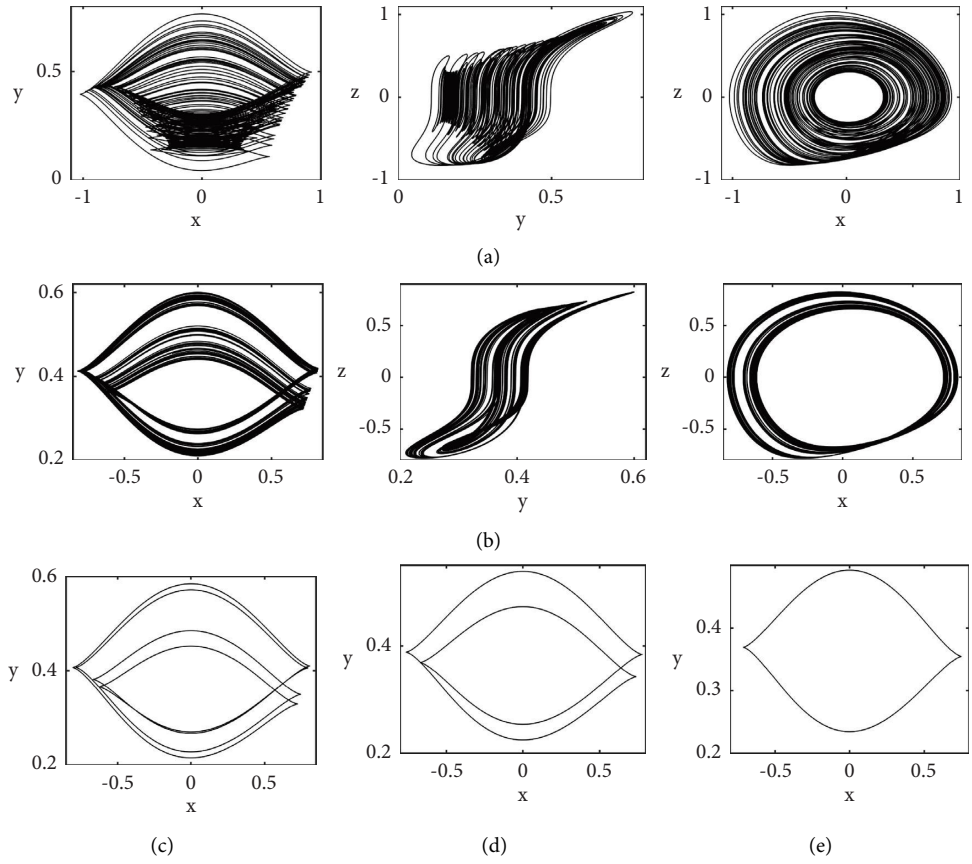

Figure 1: Projections of phase portraits of system (1a)–(1c) for different values of a: (a) $a = 3.05$, (b) $a = 3.18$, (c) $a = 3.22$, (d) $a = 3.35$, and (e) $a = 3.45$ with initial conditions $(x(0), y(0), z(0)) = (0.0, 0.1, 0.2)$.

$$\lambda\left[\lambda^2 - a\left(y^*\right)^2\lambda + 1\right] = 0. \tag{4}$$

By making use of the Routh–Hurwitz criteria, the roots of equation (4) are all real and negative if and only if $-a\left(y^*\right)^2 > 0$. Since $a > 0$, the parabolic equilibrium point E_1 is always unstable. So, the stability of the parabolic equilibrium point E_1 does not depend on the boosting controller β. In order to check the partial amplitude control of system (3a)–(3c), a plot of the average values of the state variables x, y, and z against the boosting controller β is done in Figure 2.

Figure 2 shows that an increase in the boosting controller β leads to a decrease in the average of the state variable x while the two other state variables y and z remain almost constant. The phase portraits of system (3a)–(3c) and time evolutions are depicted in Figure 3 for different values of the boosting controller β.

Figure 3(a) shows that by increasing the boosting controller β, the amplitudes of the state variable x are shifted in the left in the plane (x, y) while Figure 3(b) shows that the amplitude of the state variable x is boosted from a bipolar signal to a unipolar signal by increasing the boosting controller β. The amplitudes of system (1a)–(1c) can be totally controlled by replacing $x \longrightarrow x/\sigma, y \longrightarrow y/\sigma, z \longrightarrow z/\sigma$ into system (1a)–(1c) where σ being the scaling amplitude. So, system (1a)–(1c) becomes

$$\frac{\mathrm{d}x}{\mathrm{d}t} = -z, \tag{5a}$$

$$\frac{\mathrm{d}y}{\mathrm{d}t} = x\left(\frac{z}{\sigma}\right)^2, \tag{5b}$$

$$\frac{\mathrm{d}z}{\mathrm{d}t} = x - \frac{y^2}{\sigma} + \frac{z}{\sigma^2}\left(ay^2 - z^2\right). \tag{5c}$$

System (5a)–(5c) has $E_2 = \left\{(x, y, z) \in R^3/x = \left(y^*\right)^2/\sigma, y = y^*, z = 0\right\}$ as the parabolic equilibrium point. The characteristic equation of the parabolic equilibrium point E_2 is

$$\lambda\left[\lambda^2 - \frac{a\left(y^*\right)^2}{\sigma^2}\lambda + 1\right] = 0. \tag{6}$$

By applying the Routh–Hurwitz criteria, all the roots of equation (6) have negative real parts if and only if $-a\left(y^*\right)^2/\sigma^2 > 0$. Since $a > 0$, the parabolic equilibrium point E_2 is always unstable. So the stability of the parabolic equilibrium point E_2 is independent of the scaling amplitude σ. The phase planes of system (5a)–(5c) are depicted in Figure 4 for specific values of the scaling amplitude σ.

The amplitudes of the state variables x, y, z are increased alongside the scaling amplitude σ as shown in Figure 4.

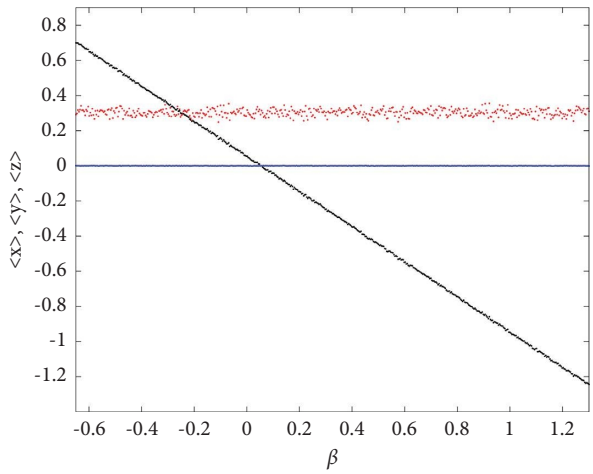

Figure 2: Average values of the state variables x (black), y (red), and z (blue) against the boosting controller β for $a = 3.05$.

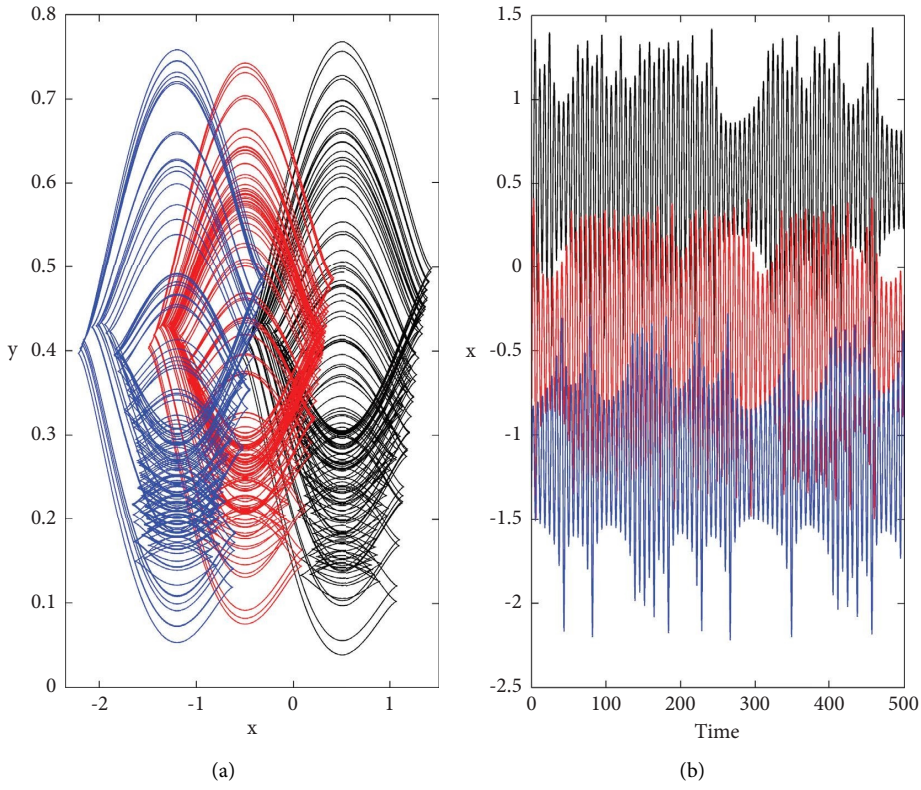

Figure 3: (a) Projections of phase portraits of system (3a)–(3c) in the plane (x, y) and (b) time evolutions of the state variable x for specific values of β: $\beta = -0.5$ (black), $\beta = 0.5$ (red), and $\beta = 1.2$ (blue). The other parameter is $a = 3.05$ for conditions $(x(0), y(0), z(0)) = (0.0, 0.1, 0.2)$.

The microcontroller implementation of 3D autonomous system with a parabolic equilibrium point is depicted in Figure 5.

Figure 5 is made of the integrated circuit ATmega328P microcontroller, the FTD232 module, and the TFT display of dimensions 800×480 connected to the microcontroller via the driver RA8875. The Runge–Kutta method order four is used in this microcontroller. The phase planes obtained from the circuit in Figure 5 point are depicted in Figure 6.

The microcontroller results of Figure 6 qualitatively agree with the numerical simulations of Figure 1.

3. Chaos Control of 3D Autonomous System with a Parabolic Equilibrium Point

The sliding mode control method is used to control chaos in 3D autonomous system with a parabolic equilibrium point in this section. The controlled system under study is described by

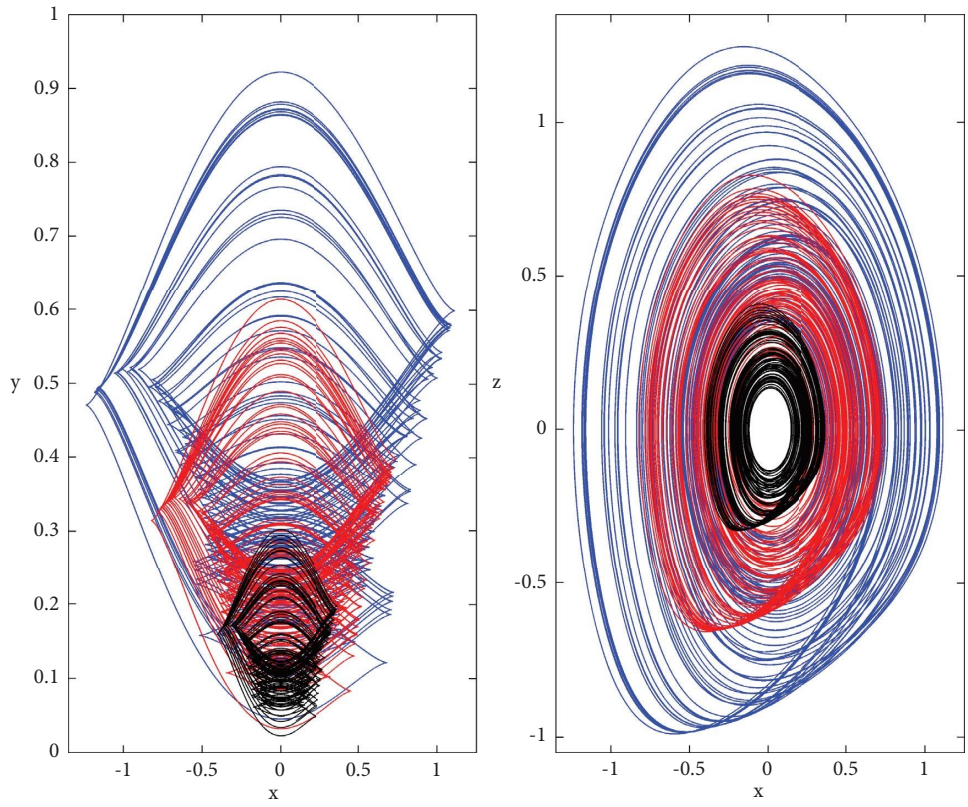

Figure 4: Projections of phase portraits in the planes (x, y) and (x, z) of system (5a)–(5c) for $a = 3.05$ and different values of scaling amplitude σ: $\sigma = 0.4$ (black), $\sigma = 0.8$ (red), and $\sigma = 1.2$ (blue); initial conditions being $(x(0), y(0), z(0)) = (0.0, 0.1, 0.2)$.

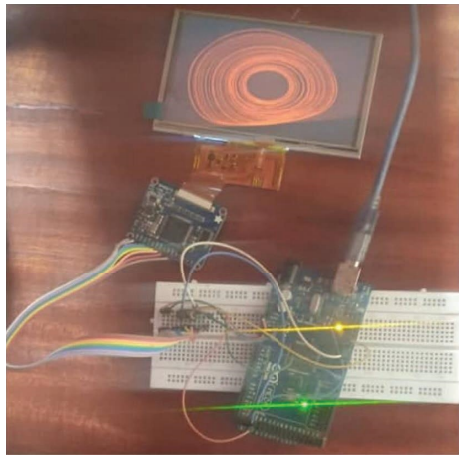

Figure 5: Microcontroller circuit of 3D autonomous system with a parabolic equilibrium point described by system (1a)–(1c).

$$\frac{dx}{dt} = -z, \tag{7a}$$

$$\frac{dy}{dt} = xz^2 + u_1, \tag{7b}$$

$$\frac{dz}{dt} = x - y^2 + z\left(ay^2 - z^2\right) + u_2. \tag{7c}$$

With $u_1 = x - y - xz^2$ and $u_2 = -[x - y^2 + z(ay^2 - z^2)] + \nu_1$ being the controllers designed based on sliding mode control method, the variable ν_1 is the new input. Thus, system (7a)–(7c) becomes

$$\frac{dx}{dt} = -z, \tag{8a}$$

$$\frac{dy}{dt} = x - y, \tag{8b}$$

$$\frac{dz}{dt} = \nu_1. \tag{8c}$$

Thence, $y \longrightarrow 0$ if $x, z \longrightarrow 0$ as $t \longrightarrow \infty$, the second order of the above system is stabilized as

$$\frac{dx}{dt} = -z, \tag{9a}$$

$$\frac{dz}{dt} = \nu_1. \tag{9b}$$

The sliding surface of system (9a) and (9b) is defined as

$$\sigma_1 = x - z \Rightarrow \frac{d\sigma_1}{dt} = -z - \nu_1. \tag{10}$$

By choosing $\nu_1 = -z + k\sigma_1$, $k > 0$, equation (10) becomes

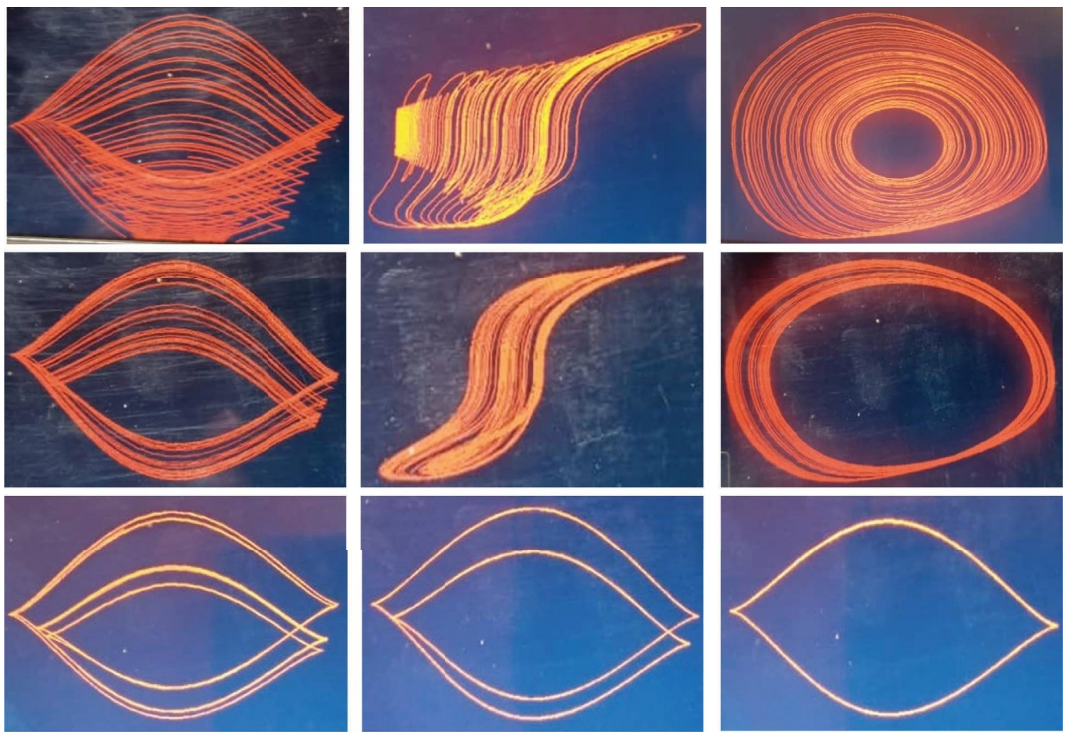

Figure 6: Projections of phase planes obtained from the microcontroller implementation of 3D autonomous system with a parabolic equilibrium point.

$$\frac{d\sigma_1}{dt} = -k\sigma_1. \tag{11}$$

System (8a)–(8c) has a single equilibrium point $O_1 = (0, 0, 0)$ with the characteristic equation:

$$\lambda^3 + (k+2)\lambda^2 + (2k+1)\lambda + k = 0. \tag{12}$$

The Routh–Hurwitz conditions for the stability of system (8a)–(8c) at the only equilibrium point $O_1 = (0, 0, 0)$ are

$$k + 2 > 0, \tag{13a}$$

$$k > 0, \tag{13b}$$

$$2k^2 + 4k + 2 > 0. \tag{13c}$$

The solution of the set of inequalities (13a)–(13c) is $k > 0$. So, system (8a)–(8c) is asymptotically stable for $k_1 > 1$. System (9a) and (9b) has a single equilibrium point $O_2 = (0, 0)$, and the characteristic equation at this equilibrium point is

$$\lambda^2 + (k+1)\lambda + k = 0. \tag{14}$$

The Routh–Hurwitz conditions for the stability of system (9a) and (9b) at the only equilibrium point $O_2 = (0, 0)$ are

$$k + 1 > 0, \tag{15a}$$

$$k > 0. \tag{15b}$$

The solution of the set of inequalities (15a) and (15b) is $k > 0$. So, system (9a) and (9b) is asymptotically stable for $k > 0$. As a result, systems (8a)–(8c) and (9a) and (9b) are asymptotically stable for $k > 0$. The state variables of controlled system (8a)–(8c) are depicted in Figure 7.

Chaos control of system (1a)–(1c) by using the sliding mode control method is efficient as revealed by the numerical simulation results depicted in Figure 7.

4. Synchronization of Chaotic 3D Autonomous Systems by Using the Same or Different Parameters

In this section, the synchronization of the 3D autonomous systems with a parabolic equilibrium point is studied by using unidirectional feedback linear and nonlinear coupling terms. The drive 3D autonomous system with a parabolic equilibrium point is given by

$$\frac{dx_1}{dt} = -z_1, \tag{16a}$$

$$\frac{dy_1}{dt} = x_1 z_1^2, \tag{16b}$$

$$\frac{dz_1}{dt} = x_1 - y_1^2 + z_1\left(a_1 y_1^2 - z_1^2\right), \tag{16c}$$

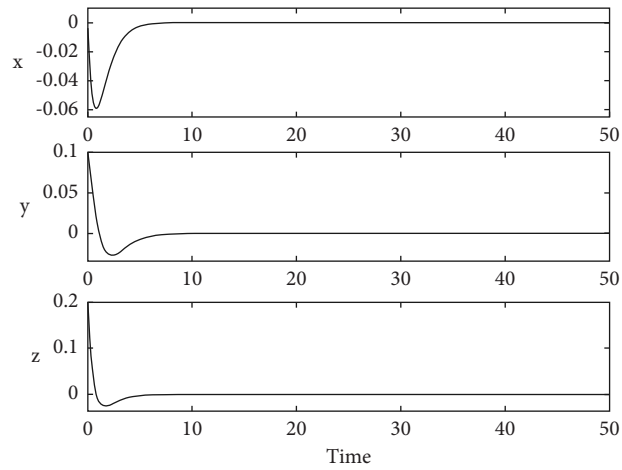

Figure 7: Time evolutions of controlled x, y, z for $k = 1.5$ and $a = 3.05$ with initial conditions being $(x(0), y(0), z(0)) = (0, 0.1, 0.2)$.

where a_1 is a value that assures chaotic behavior and the response 3D autonomous system with a parabolic equilibrium given by

$$\frac{dx_2}{dt} = -z_2 + u_1, \tag{17a}$$

$$\frac{dy_2}{dt} = x_2 z_2^2 + u_2, \tag{17b}$$

$$\frac{dz_2}{dt} = x_2 - y_2^2 + z_2\left(a_2 y_2^2 - z_2^2\right) + u_3. \tag{17c}$$

With a_2 being the parameter whose value assures chaotic behavior, the vector $U = (u_1, u_2, u_3)^T$ is a controller vector. Since the 3D autonomous system with a parabolic equilibrium point has two different shapes of chaotic attractors, it is interesting to study the synchronization between identical unidirectionally coupled 3D autonomous systems with a parabolic equilibrium point by using each shape of chaotic attractors and between two identical unidirectionally coupled 3D autonomous systems with a parabolic equilibrium by using different shapes of chaotic attractors. The subsection that follows presents the achievement of the synchronization between two 3D proposed systems with the same parameters using the unidirectional linear feedback coupling scheme.

4.1. Synchronization of Proposed Chaotic Systems with the Same Parameters by Using Unidirectional Linear Feedback Coupling. Here, the drive and response systems (16a)–(16c) and (17a)–(17c) are coupled by using the unidirectional linear feedback coupling: $u_1 = k_1(x_1 - x_2)$, $u_2 = k_2 \quad (y_1 - y_2), u_3 = k_3(z_1 - z_2)$ with the constant parameters k_1, k_2, and k_3 being the coupling strengths. For easy analysis, only the linear feedback coupling u_2 is used for the coupling of the two identical chaotic systems. The maximum synchronization error $e_{\max} = \mathrm{Max}(\sqrt{(x_1 - x_2)^2 + (y_1 - y_2)^2 + (z_1 - z_2)^2})$ and the transverse Lyapunov exponents are to estimate the quality of synchronization between the trajectories of the response and drive systems. The plots of the largest transverse Lyapunov exponents and the maximum synchronization error $e_{\max}$ as a function of the coupling strength k_2 are depicted in Figure 8.

The response and drive systems are synchronized, if the maximum synchronization error becomes approximately equal to zero. From the left panel of Figure 8(a), one can see that the response and drive systems are synchronized in the chaotic regime (with $a_1 = a_2 = 3.05$) for $0.12 \le k_2 \le 0.4$. The boundary and the stability of synchronization are attested by the largest transverse Lyapunov exponent shown in the left panel of Figure 8(b). The response and drive systems are synchronized in the chaotic regime (with $a_1 = a_2 = 3.18$) for $0.17 \le k_2 \le 0.35$ (see the right panel of Figure 8(a)). The boundary and the stability of synchronization are confirmed by the largest transverse Lyapunov exponent shown in the right panel of Figure 8(b). The projection of the phase space trajectories of the response and drive systems for a given value of the coupling strength k_2 and the parameter values a_1, a_2 are plotted in Figure 9.

The drive and response systems (16a)–(16c) and (17a)–(17c) are synchronized in the two different shapes of chaotic attractors as shown in Figures 9(a) and 9(b), respectively. Worth noting is the fact that the synchronization between the drive and response systems (16a)–(16c) and (17a)–(17c) with different parameters ($a_1 = 3.05$ and $a_2 = 3.18$ or $a_1 = 3.18$ and $a_2 = 3.05$) is not achieved by using the unidirectional linear feedback coupling. In the next subsection, it is possible to achieve synchronization of identical proposed chaotic systems with different parameters by using nonlinear error feedback coupling.

4.2. Synchronization of Chaotic Systems with Different Parameters through Nonlinear Feedback Coupling. Here, the drive and response systems (16a)–(16c) and (17a)–(17c) are considered where the controller U is an active control function to be designed by using a Lyapunov exponent function. Hereafter, the controller U for which the chaos synchronization of two proposed chaotic systems with different parameters can be achieved has to be designed. For this reason, the error dynamical variable between drive system (16a)–(16c) and response system (17a)–(17c) can be written as follows:

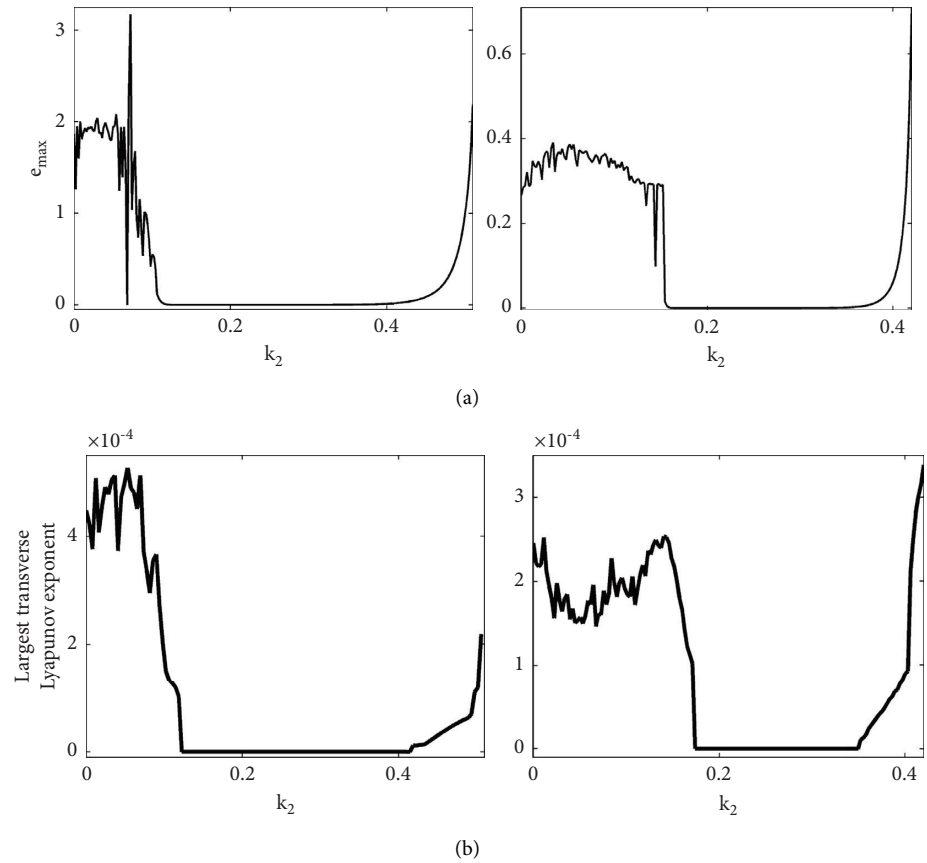

FIGURE 8: (a) Maximum synchronization error e_{max} and (b) largest transverse Lyapunov exponents against the coupling strength k_2 by using the parameter values $a_1 = a_2 = 3.05$ in the left panel and $a_1 = a_2 = 3.18$ in the right panel with $k_1 = k_3 = 0$.

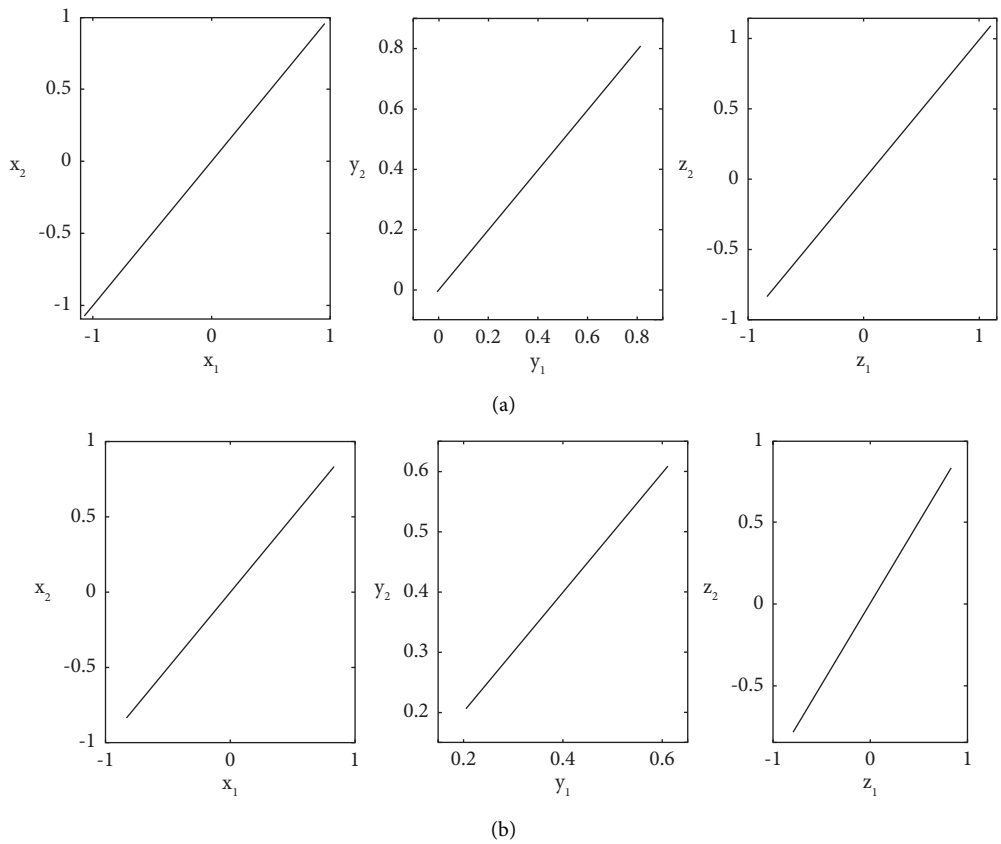

FIGURE 9: Projection of the phase space trajectories of the drive and response systems for a specific value of the coupling strength k_2, a_1 and a_2: (a) $k_2 = 0.2$, $a_1 = a_2 = 3.05$ and (b) $k_2 = 0.2$, $a_1 = a_2 = 3.18$.

$$\frac{de_x}{dt} = -e_z + u_1, \tag{18a}$$

$$\frac{de_y}{dt} = e_x z_2^2 + e_z x_1 (z_1 + z_2) + u_2, \tag{18b}$$

$$\frac{de_z}{dt} = e_x - e_y (y_1 + y_2) + e_z x_1 (z_1 + z_2) - e_z\left(z_1^2 + z_1 z_2 + z_2^2\right) - a_1 z_1 y_1^2 + a_2 z_2 y_2^2 + u_3. \tag{18c}$$

$$\frac{de_x}{dt} = -e_z + u_1, \tag{19a}$$

$$\frac{de_y}{dt} = e_x z_2^2 + e_z x_1 (z_1 + z_2) + u_2, \tag{19b}$$

$$\frac{de_z}{dt} = e_x - e_y (y_1 + y_2) + e_z x_1 (z_1 + z_2) - e_z\left(z_1^2 + z_1 z_2 + z_2^2\right) - a_1 z_1 y_1^2 + a_2 z_2 y_2^2 + u_3. \tag{19c}$$

With $e_x = x_2 - x_1$, $e_y = y_2 - y_1$, and $e_z = z_2 - z_1$, the Lyapunov function

$$L = \frac{\left(e_x^2 + e_y^2 + e_z^2\right)}{2}, \tag{20}$$

has the derivative

$$\frac{dL}{dt} = e_x (-e_z + u_1) + e_y\left[e_x z_2^2 + e_z x_1 (z_1 + z_2) + u_2\right] + e_z\left[e_x - e_y (y_1 + y_2) - e_z\left(z_1^2 + z_1 z_2 + z_2^2\right) - a_1 z_1 y_1^2 + a_2 z_2 y_2^2 + u_3\right]. \tag{21}$$

A trivial choice of $U = (u_1, u_2, u_3)^T$ is

$$\begin{aligned} u_1 &= 0, \\ u_2 &= -e_x z_2^2 - e_z x_1 (z_1 + z_2) - p_1^2 e_y, \\ u_3 &= e_y (y_1 + y_2) + e_z\left(z_1^2 + z_1 z_2 + z_2^2\right) + a_1 z_1 y_1^2 - a_2 z_2 y_2^2 - p_2^2 e_z, \end{aligned} \tag{22}$$

where p_1 and p_2 are real parameters. Then, Equation (21) becomes

$$\frac{dL}{dt} = -p_1^2 e_y^2 - p_2^2 e_z^2 < 0. \tag{23}$$

By inserting equation (22) into equations (19a)–(19c), the error system (19a)–(19c) becomes

$$\frac{de_x}{dt} = -e_z, \tag{24a}$$

$$\frac{de_y}{dt} = -p_1^2 e_y, \tag{24b}$$

$$\frac{de_z}{dt} = e_x - p_2^2 e_z. \tag{24c}$$

System (24a)–(24c) has a single equilibrium point $O_3(0, 0, 0)$ whose characteristic equation is

$$\lambda^3 + \left(p_1^2 + p_2^2\right)\lambda^2 + \left(1 + p_1^2 p_2^2\right)\lambda + p_1^2 = 0. \tag{25}$$

The Routh–Hurwitz conditions for stability reveal that the zero solution of system (24a)–(24c) is locally asymptotically stable for any values of p_1 and p_2. By choosing $p_1 = 0.5$ and $p_2 = 1$ with $a_1 = 3.0$ and $a_2 = 3.16$, the synchronization errors between the drive and response systems (16a)–(16c) and (17a)–(17c) are plotted in Figure 10.

Figure 10 reveals that the drive-response systems (16a)–(16c) and (17a)–(17c) are asymptotically synchronized after a certain period of time.

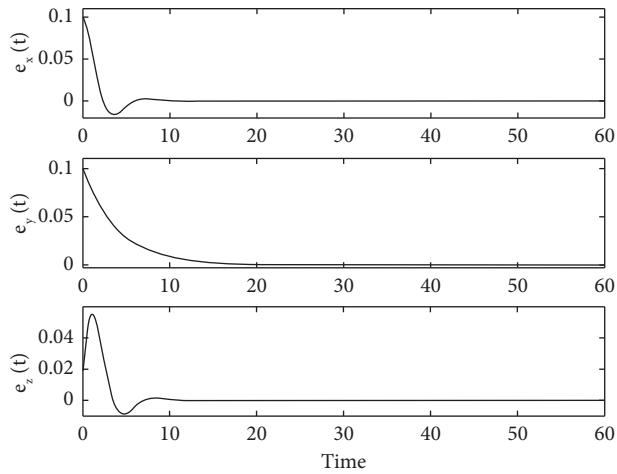

FIGURE 10: Synchronization errors between the drive-response systems (16a)–(16c) and (17a)–(17c) by using the controllers (10) for $a_1 = 3.05$, $a_2 = 3.18$, $p_1 = 0.50$, and $p_2 = 1.0$.

5. Conclusion

This paper dealt with the microcontroller implementation, controls, and synchronization of a three-dimensional chaotic autonomous system with a parabolic equilibrium point. It was found that the system exhibited periodic oscillations and two different shapes of hidden chaotic attractors. The addition of new parameters in the rate equations of this system made the partial and total amplitude controls possible. Then, the microcontroller implementation of a chaotic autonomous system with a parabolic equilibrium was realized, and the comparison between the microcontroller implementation and numerical simulations results showed a good qualitative agreement. Moreover, the sliding mode controllers were designed in order to control chaos in the three-dimensional autonomous system with a parabolic equilibrium point. The effectiveness of these designed controllers was confirmed by the numerical simulation results. Finally, the chaos synchronization of two chaotic autonomous systems with the same parameters and different initial conditions was achieved by using a unidirectional linear feedback coupling scheme. By using unidirectional nonlinear feedback coupling, it was demonstrated analytically and numerically that two chaotic autonomous systems with different parameters can synchronize.

Data Availability

The data used to support the findings of this study are included within the article.

Conflicts of Interest

The authors declare that they have no conflicts of interest.

References

[1] S. Jafari, J. C. Sprott, and F. Nazarimehr, "Recent new examples of hidden attractors," *The European Physical Journal - Special Topics*, vol. 224, no. 8, pp. 1469–1476, 2015.

[2] C. Liu, T. Liu, L. Liu, and K. Liu, "A new chaotic attractor," *Chaos, Solitons & Fractals*, vol. 22, no. 5, pp. 1031–1038, 2004.

[3] W. Zhou, Y. Xu, H. Lu, and L. Pan, "On dynamics analysis of a new chaotic attractor," *Physics Letters A*, vol. 372, no. 36, pp. 5773–5777, 2008.

[4] Q. Lai, Z. Wan, P. D. Kamdem Kuate, and H. Fotsin, "Coexisting attractors, circuit implementation and synchronization control of a new chaotic system evolved from the simplest memristor chaotic circuit," *Communications in Nonlinear Science and Numerical Simulation*, vol. 89, Article ID 105341, 2020.

[5] S. Nag Chowdhury and D. Ghosh, "Hidden attractors: a new chaotic system without equilibria," *The European Physical Journal - Special Topics*, vol. 229, no. 6-7, pp. 1299–1308, 2020.

[6] V. T. Pham, S. Jafari, C. Volos, and T. Kapitaniak, "A gallery of chaotic systems with an infinite number of equilibrium points," *Chaos, Solitons & Fractals*, vol. 93, pp. 58–63, 2016.

[7] L. H. Gong, H. X. Luo, R. Q. Wu, and N. R. Zhou, "New 4D chaotic system with hidden attractors and self-excited attractors and its application in image encryption based on RNG," *Physica A: Statistical Mechanics and Its Applications*, vol. 591, Article ID 126793, 2022.

[8] V. T. Pham, C. K. Volos, S. Vaidyanathan, S. Jafari, P. M. Gokul, and T. Kapitaniak, "Chaos in a system with parabolic equilibrium," in *Recent Advances in Chaotic Systems and Synchronization*, pp. 41–61, Academic Press, Cambridge, MA, USA, 2019.

[9] R. Karthikeyan and V. Sundarapandian, "Hybrid chaos synchronization of four–scroll systems via active control," *Journal of Electrical Engineering*, vol. 65, no. 2, pp. 97–103, 2014.

[10] M. Srivastava, S. P. Ansari, S. K. Agrawal, S. Das, and A. Y. T. Leung, "Anti-synchronization between identical and non-identical fractional-order chaotic systems using active control method," *Nonlinear Dynamics*, vol. 76, no. 2, pp. 905–914, 2014.

[11] S. T. Kingni, A. Cheukem, P. R. N. Tuwa, A. C. Chamgoué, V. T. Pham, and S. Jafari, "Synchronous reluctance motor with load vibration perturbation: analysis, electronic implementation and adaptive backstepping sliding mode control," *Iranian Journal of Science and Technology, Transactions of Electrical Engineering*, vol. 45, no. 2, pp. 645–654, 2021.

[12] S. Vaidyanathan and C. H. Lien, *Applications of Sliding Mode Control in Science and Engineering*, Springer, Heidelberg, Germany, 2017.

[13] M. Yassen, "Adaptive control and synchronization of a modified Chua's circuit system," *Applied Mathematics and Computation*, vol. 135, no. 1, pp. 113–128, 2003.

[14] S. Vaidyanathan and A. T. Azar, "Generalized projective synchronization of a novel hyperchaotic four-wing system via adaptive control method," in *Advances in Chaos Theory and Intelligent Control*, pp. 275–296, Springer, Heidelberg, Germany, 2016.

[15] E. D. Dongmo, K. S. Ojo, P. Woafo, and A. N. Njah, "Difference synchronization of identical and nonidentical chaotic and hyperchaotic systems of different orders using active backstepping design," *Journal of Computational and Nonlinear Dynamics*, vol. 13, no. 5, pp. 051005–051013, 2018.

[16] E. D. Dongmo, K. S. Ojo, P. Woafo, and A. N. Njah, "Difference-difference synchronizations of chaotic and hyperchaotic systems," *Journal of Applied Nonlinear Dynamics*, vol. 11, no. 2, pp. 487–497, 2022.

[17] L. M. Pecora and T. L. Carroll, "Synchronizing chaotic circuits," in *Nonlinear Dynamics in Circuits*, pp. 215–248, World Scientifi, Singapore, 1995.

[18] J. Ma, F. Li, L. Huang, and W. Y. Jin, "Complete synchronization, phase synchronization and parameters estimation in a realistic chaotic system," *Communications in Nonlinear Science and Numerical Simulation*, vol. 16, no. 9, pp. 3770–3785, 2011.

[19] G. M. Mahmoud and E. E. Mahmoud, "Complete synchronization of chaotic complex nonlinear systems with uncertain parameters," *Nonlinear Dynamics*, vol. 62, no. 4, pp. 875–882, 2010.

[20] H. D. I. Abarbanel, N. F. Rulkov, and M. M. Sushchik, "Generalized synchronization of chaos: the auxiliary system approach," *Physical Review*, vol. 53, no. 5, pp. 4528–4535, 1996.

[21] S. Vaidyanathan and S. Sampath, "Anti-synchronization of four-wing chaotic systems via sliding mode control," *International Journal of Automation and Computing*, vol. 9, no. 3, pp. 274–279, 2012.

[22] J. Yan and C. Li, "Generalized projective synchronization of a unified chaotic system," *Chaos, Solitons & Fractals*, vol. 26, no. 4, pp. 1119–1124, 2005.

[23] K. Sebastian Sudheer and M. Sabir, "Hybrid synchronization of hyperchaotic Lu system," *Pramana*, vol. 73, no. 4, pp. 781–786, 2009.

[24] H. N. Agiza and M. Yassen, "Synchronization of Rossler and Chen chaotic dynamical systems using active control," *Physics Letters A*, vol. 278, no. 4, pp. 191–197, 2001.